Human bone perivascular niche-on-a-chip for studying metastatic colonization

Alessandro Marturano-Kruik[a,b], Michele Maria Nava[b], Keith Yeager[a], Alan Chramiec[a], Luke Hao[a], Samuel Robinson[a], Edward Guo[a], Manuela Teresa Raimondi[b,1], and Gordana Vunjak-Novakovic[a,c,1]

[a]Department of Biomedical Engineering, Columbia University, New York, NY 10032; [b]Department of Chemistry, Materials and Chemical Engineering "G Natta," Politecnico di Milano, 20133 Milan, Italy; and [c]Department of Medicine, Columbia University, New York, NY 10032

Edited by Kristi S. Anseth, University of Colorado Boulder, Boulder, CO, and approved December 22, 2017 (received for review August 12, 2017)

Eight out of 10 breast cancer patients die within 5 years after the primary tumor has spread to the bones. Tumor cells disseminated from the breast roam the vasculature, colonizing perivascular niches around blood capillaries. Slow flows support the niche maintenance by driving the oxygen, nutrients, and signaling factors from the blood into the interstitial tissue, while extracellular matrix, endothelial cells, and mesenchymal stem cells regulate metastatic homing. Here, we show the feasibility of developing a perfused bone perivascular niche-on-a-chip to investigate the progression and drug resistance of breast cancer cells colonizing the bone. The model is a functional human triculture with stable vascular networks within a 3D native bone matrix cultured on a microfluidic chip. Providing the niche-on-a-chip with controlled flow velocities, shear stresses, and oxygen gradients, we established a long-lasting, self-assembled vascular network without supplementation of angiogenic factors. We further show that human bone marrow-derived mesenchymal stem cells, which have undergone phenotypical transition toward perivascular cell lineages, support the formation of capillary-like structures lining the vascular lumen. Finally, breast cancer cells exposed to interstitial flow within the bone perivascular niche-on-a-chip persist in a slow-proliferative state associated with increased drug resistance. We propose that the bone perivascular niche-on-a-chip with interstitial flow promotes the formation of stable vasculature and mediates cancer cell colonization.

metastatic colonization | bone perivascular niche | breast cancer | drug resistance | microfluidic chip

Disseminated tumor cells can emerge as bone metastases after years or decades of latency, killing breast cancer patients (1, 2). Elucidating the cellular mechanisms and the role of the tumor microenvironment in regulating this latency is crucial for improving survival rates through targeted therapy. Recent evidence shows that cancer cells escaping the vasculature colonize specific niches around blood capillaries in the bone marrow—known as perivascular niches (3). Here, the endothelium, stem cells, and the extracellular matrix (ECM) modulate cancer cell survival. Slow flows driving oxygen, nutrients, and signaling factors from the blood vessels into the interstitial tissue are key players in the niche maintenance (4). While in vivo models have helped identify tumor cells residing in the perivascular niches, manipulating the host microenvironment to study the contribution of niche components remains challenging (5). Using engineering techniques, the cells, ECM, and biophysical signals can be controlled in vitro. For example, endothelial cells (ECs) mixed with stromal cells in a 3D hydrogel provided insights on how vascular sprouts mediate breast cancer growth (6). Similar systems can be matured on microfluidic chips to form tissues with organ-like features—also known as organs-on-a-chip. Crucial steps of tumor angiogenesis, migration, and extravasation have been successfully recapitulated using these models (7–10). However, one main limitation of the existing models is the need for high concentrations of growth and angiogenic factors to promote vascular sprouting. In the growth-promoting milieu, it is challenging to mimic early metastatic events and cancer latency because of unchecked cancer cell proliferation. Most of the previously established models rely on passive diffusion of molecules, whereas flows in vivo regulate the balance between nutrient supply and metabolite removal. Soft hydrogels are highly effective in promoting vascular formation but fail to mimic the stiffness and biochemical composition of native bone niche. Here, we addressed some limitations of the existing models by developing a bone perivascular (BoPV) niche-on-a-chip incorporating interstitial flow to investigate breast cancer metastatic colonization and drug resistance. To establish the model, human endothelial and bone marrow-derived mesenchymal stem cells (MSCs) were cultured in a native bone matrix and placed into a microfluidic chip, where cells were exposed to fluid flow. By infusing breast cancer cells, we mimicked metastatic colonization using a functional human triculture system. Exposing cells to physiologically relevant flow velocities and oxygen gradients, we achieved a long-lasting, self-assembled microvascular network without continuous supplementation of angiogenic factors. The phenotypical transition of MSCs toward mural cell lineages supported the formation of capillary-like structures in the niche. Finally, disseminated breast cancer cells exposed to flow exhibited a slow-proliferative state and increased drug resistance in the BoPV niche-on-a-chip model.

Results

Three-Dimensional Vascular Networks in Bone. Despite advances in modeling cancer metastasis, the maintenance of vascular networks in vitro still requires continuous use of specialized culture mediums. Under these conditions, cancer cells are forced to grow regardless of the niche signaling. We hypothesized that

Significance

Improved human preclinical models are needed to better predict patients' responses to anticancer drugs. Increasing the complexity of models may be a successful strategy only if crucial components of a tumor are identified, replicated, and controlled in vitro. We developed a perivascular niche to study metastatic colonization of the bone. Using a microfluidic chip, we exposed the niche to interstitial flow, oxygen gradients, and external forces, and established a dense vascular network. Cancer cells colonizing the bone resisted targeted therapy by entering a slow proliferative state. We expect that microfluidic niche-on-chip models will facilitate the development of drugs targeting persistent tumor cells into the bone and help manage the risk of metastatic relapse.

Author contributions: A.M.-K. and G.V.-N. designed research; A.M.-K., M.M.N., K.Y., A.C., L.H., S.R., and E.G. performed research; A.M.-K., M.M.N., and G.V.-N. analyzed data; and A.M.-K., M.T.R., and G.V.-N. wrote the paper.

The authors declare no conflict of interest.

This article is a PNAS Direct Submission.

[1]To whom correspondence may be addressed. Email: manuela.raimondi@polimi.it or gv2131@columbia.edu.

This article contains supporting information online at www.pnas.org/lookup/suppl/doi:10.1073/pnas.1714282115/-/DCSupplemental.

using a 3D bone scaffold, with the preserved native biochemical and biophysical composition, will support the formation of stable microvasculature without high concentrations of angiogenic or growth factors commonly needed in vitro. To test this hypothesis, we seeded fluorescently labeled ECs mixed with MSCs into decellularized 3D bone matrix and two controls: 2D (monolayer) and 3D polystyrene (commonly used plastic for cell culture dishes). Bone decellularization was carried out before repopulating the matrix with human cells. To demonstrate effectiveness of the decellularization protocol, we measured the DNA content of the bone before and after decellularization (430.6 ± 150 and 7.3 ± 1.5 ng of DNA per mg of tissue's wet weight, respectively) (*SI Appendix*, Fig. S1*A*). A micro-computed tomography (μ-CT) scan showed the retention of the mineralized trabecular structure while all cellular material was removed (*SI Appendix*, Fig. S1*B*). To document the maintenance of ECM components, we measured the milligrams of hydroxyapatite per unit volume (tissue mineral density), within the ranges reported for humans (*SI Appendix*, Fig. S1*C*) (11). The trabecular voids were filled with the MSCs–ECs coculture and maintained for 1 wk in endothelial medium (EM) followed by 1 wk in serum-reduced medium (SRM) (Fig. 1 *A* and *B*). Controls were maintained in EM for 14 d. Using live confocal imaging, we measured vascular formation and quantified vessel density, number of junctions, total vessel length, average vessel length, and number of endpoints (Fig. 1 *C* and *D* and *SI Appendix*, Fig. S2 *A–D*). ECs maintained in SRM in 2D and 3D polystyrene cultures generated shorter vessels compared with those grown in EM. In the bone matrix, ECs failed to organize vascular connections when maintained in EM for 2 wk. Switching to SRM after the first week of culture induced the formation of vascular networks with increased branching, number of junctions, and total and average vessel length. By analyzing the mRNA levels of genes involved in vasculogenesis, we found increased *TSP1*, *VEGFR1*, *VEGFR2*, *POSTN*, and *Survivin* expression in cells cultured in SRM (Fig. 1*E*). We observed higher *VEGFR1*, *VEGFR2*, *POSTN*, and lower *TSP1* expression in the coculture compared with the MSCs-only culture. However, in the absence of flow, vascular networks were confined to the outer edges of the bone and relied on diffusional mass transport only.

Microfluidic Niche-on-a-Chip. Because the MSCs–ECs cultured statically formed vascular networks only at the outer edges of the bone matrix, we investigated whether physiologically relevant interstitial flow would support the formation of vascular networks throughout the bone tissue. To this end, the tissues were placed into the microfluidic chip, cultured in SRM, and exposed to controlled flow velocities for 1 wk to form the BoPV niche-on-a-chip (Fig. 1*F*). The perfusion chambers of the chip supported three independent samples. The chambers were sealed by placing a glass coverslip on top of the flow gasket and secured using

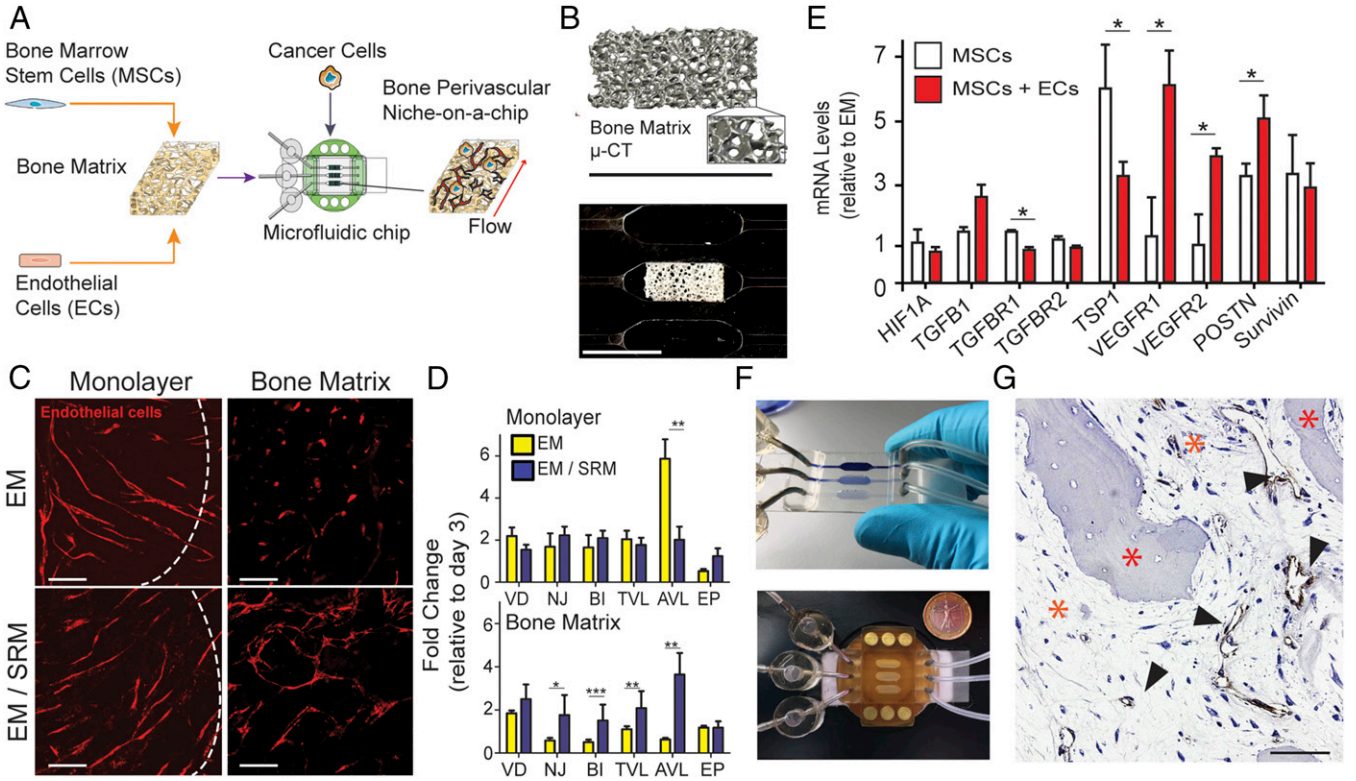

Fig. 1. Formation and maintenance of the niche-on-a-chip. (*A*) Generation of the bone perivascular (BoPV) niche for studies of breast cancer colonization. Human bone marrow-derived mesenchymal stem cells (MSCs) and endothelial cells (ECs) were cultured in monolayers and in 3D decellularized bone matrix. Culture regimen involved 1 wk in endothelial medium (EM) followed by 1 wk in serum-reduced medium (SRM), or 2 wk in EM. After 1 wk of static culture, cancer cells were infused into the bone tissue, and perfusion was initiated in the microfluidic chip. (*B*, *Top*) Bone tissue reconstruction based on micro-computed tomography (μ-CT) data. (*Bottom*) Rectangular-shaped bone matrix in the microfluidic chip. (*C*) Confocal images of RFP-labeled ECs forming vascular networks in monolayers or in the bone matrix. (Scale bar: 200 μm.) (*D*) Quantification of neovessel formation using confocal images. Vessel density (VD), number of junctions (NJ), branching index (BI), total vessel length (TVL), average vessel length (AVL), and number of endpoints (EP) were measured after 2 wk of culture and normalized to day 3 values. (*E*) Gene expression of MSCs-only or MSCs-plus-ECs cultures in the bone matrix. mRNA levels were normalized to the gene expression levels after 2 wk of culture in EM. (*F*) Overview of the microfluidic chip used to culture the BoPV niche. (*G*) Immunostaining of endothelial marker CD31 in the BoPV niche-on-a-chip, showing capillary-like structures (arrowheads) filling the trabecular pores (green asterisk) in the preexisting bone trabeculae (red asterisks). (Scale bar: 50 μm.) Data in *D* and *E* are represented as average + SD; $*P < 0.05$; $**P < 0.01$; $***P < 0.001$; unpaired two-tailed Student's *t* test.

magnetic clamps. The device is optically accessible, allowing assessment of cell/tissue outcomes in real time. Syringes containing fresh culture medium were connected to the inlet loop through bubble traps, and a glass container was used to collect waste medium (*SI Appendix*, Fig. S2*E* and Movie S1). Immunohistochemistry showed that, after 2 wk of culture, MSCs and ECs populated the trabecular space. CD31-negative MSCs cells lined the bone trabeculae promoting tissue integration with the existing mineral matrix, whereas CD31-positive ECs formed capillary-like structures within the trabecular pores (Fig. 1*G*).

Optimization of Interstitial Flow Velocities and Shear Forces. Interstitial flows within 0.1–5 $\mu m \cdot s^{-1}$ enable nutrient supply in vivo and impart extracellular forces on cells regulating tissue morphogenesis (4). To finely tune the perfusion flow within the BoPV niche, we used a computational fluid dynamics (CFD) approach (Fig. 2*A* and Movie S2). To account for the complex geometrical features of trabecular bone, we imported the μ-CT of the bone scaffold in the CFD software (*SI Appendix*, Fig. S3 *A* and *B*, and Table S1). In the computational model, we tested several flow rates and found that 0.25 $\mu L \cdot min^{-1}$ flow rate resulted in an average fluid velocity of ~3.1 $\mu m \cdot s^{-1}$ within the 3D bone matrix (Fig. 2*B*). To validate the CFD analysis, fluorescent microbeads were perfused through the bone tissue at different flow rates (Fig. 2*C* and Movies S3 and S4). The microbead displacement across frames was recorded using a fluorescent microscope and analyzed using micro-particle image velocimetry (μ-PIV) software. No significant difference was found between the CFD-predicted and the μ-PIV–measured velocity values, suggesting that the computational analysis accurately predicted the fluid dynamics in the 3D structure (Fig. 2*D*). The 0.25 $\mu L \cdot min^{-1}$ resulting in an average interstitial fluid velocity of ~3.1 $\mu m \cdot s^{-1}$ was used in all of the following experiments, unless specified otherwise. Because specific thresholds of fluid-derived shear forces can drive cellular responses including endothelial sprouting, cancer cell migration, and growth inhibition (12, 13), we used the CFD to estimate the shear stress acting on the bone tissues at different flow velocities (Fig. 2 *E* and *F*). The shear stresses estimated for 0.25 $\mu L \cdot min^{-1}$ ranged between 0.03 and 0.32 mPa, and peaks of force were observed in areas with higher flow velocities (Fig. 2*G* and *SI Appendix*, Fig. S4). Our computational and experimental approach enabled fine-tuning of flow

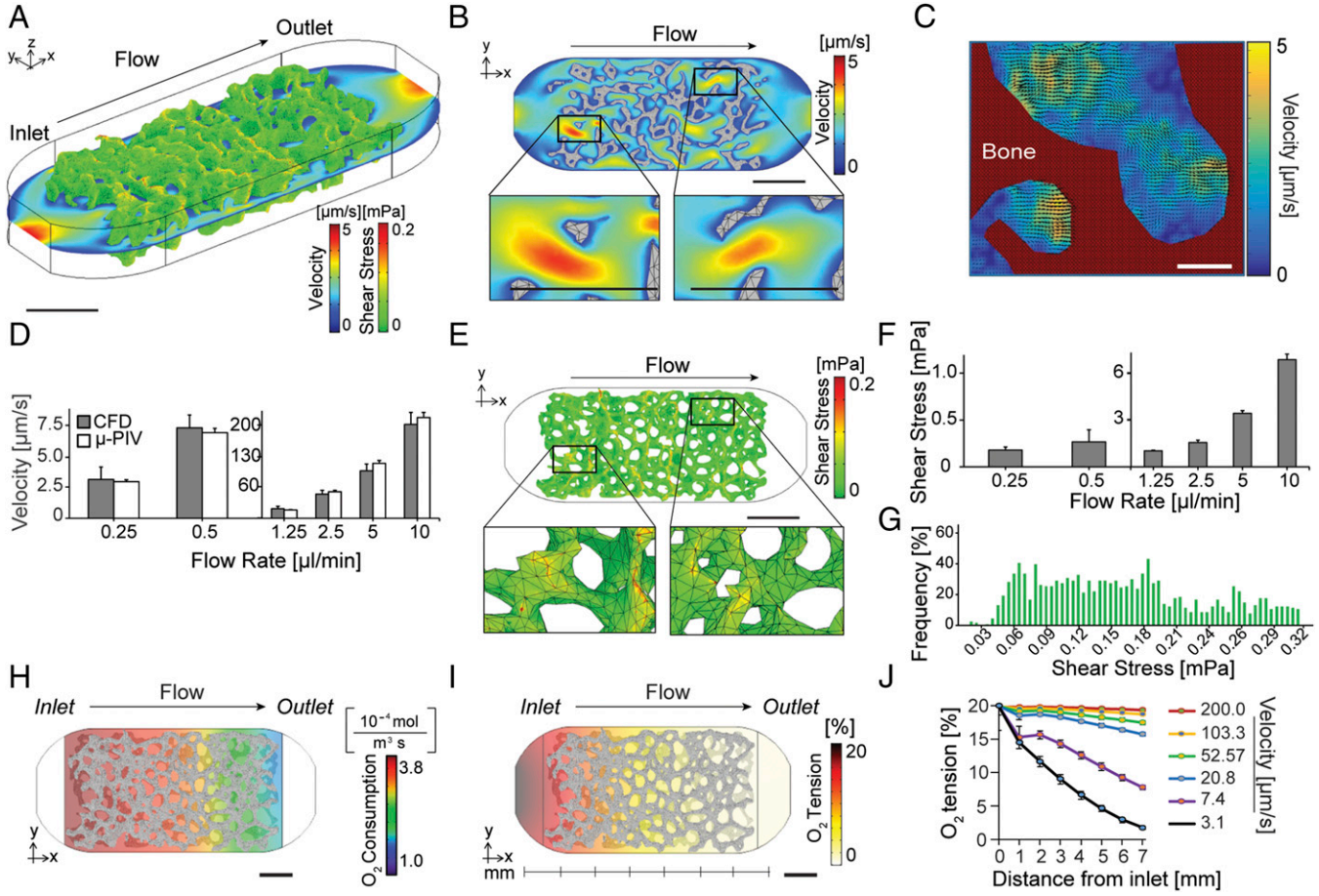

Fig. 2. Flow velocity, shear stress, and oxygen profiles in the BoPV niche-on-a-chip. (*A*) Color maps showing bone μ-CT scans imported in a CFD software for the prediction of flow velocities and shear stresses at an inlet flow rate of 0.25 $\mu L \cdot min^{-1}$. (Scale bar: 1 mm.) (*B*) Color maps of the flow velocity at low (*Top*) and high magnification (*Bottom*). (Scale bar: 1 mm.) (*C*) Validation of the CFD-predicted flow velocities, using fluorescent microspheres suspended in culture medium and perfused through the bone tissue. The microspheres were tracked and the average flow velocity was calculated using micro-particle image velocimetry (μ-PIV) software. (Scale bar: 50 μm.) (*D*) Comparison of the measured (μ-PIV) and CFD-predicted velocities in the bone matrix at different inlet flow rates. An inlet flow rate of 0.25 $\mu L \cdot min^{-1}$ resulted in an interstitial fluid velocity of ~3.1 $\mu m \cdot s^{-1}$. (*E*) Color maps of the shear stress in the bone matrix. (Scale bar: 1 mm.) (*F*) Shear stress magnitude in the bone tissue at different inlet flow rates. (*G*) Histogram of the shear stress magnitude and frequency in the perfused BoPV niche at an average velocity of ~3.1 $\mu m \cdot s^{-1}$. (*H* and *I*) Estimated oxygen consumption (*H*) and concentration (*I*) in the BoPV niche after 2 wk of culture. Color maps in isometric view (*Top*) and top view (*Bottom*). (Scale bar: 1 mm.) (*J*) Predicted oxygen depletion in the BoPV niche at week 2, a function of the distance from the flow inlet and the flow velocity (~3.1 $\mu m \cdot s^{-1}$). (Scale bar: 3 mm.) Data in *D* and *F* are shown as average + SD; $n = 3$.

rates in the microfluidic device to achieve controlled interstitial flow velocities within the niche-on-a-chip.

Flow-Controlled Oxygen Concentration Profiles. Oxygen gradients regulate stem cell homing and cancer progression in the bone (14, 15). Using a computational analysis that has been validated by previously reported experimental measurements (16), we studied how flow velocities regulated oxygen profiles in the BoPV niche-on-a-chip. The perfusion chamber was designed to force medium flow through the front (inlet) and the back (outlet) surface of the rectangular bone tissue (Fig. 2 *H* and *I*). The gradients in the perfused tissue model resulted from the diffusive and convective transport of oxygen coupled to its consumption by cells. In the perfused niche, oxygen concentration decreased along the scaffold length, in the direction of flow. An interstitial velocity of ~3.1 $\mu m \cdot s^{-1}$ resulted in a steep decrease in oxygen concentrations of 75% across the length of the tissue (Fig. 2*J*). As expected, higher flow rates resulted in shallower gradients, due to the increased oxygen supply at relatively unchanged cellular consumption. Controlled perfusion, mimicking native interstitial flow, was critical for the transport of nutrients, metabolites, and oxygen throughout the tissue volume.

BoPV Niche-on-a-Chip with Interstitial Flow. Immunostaining showed that interstitial flow (~3.1 $\mu m \cdot s^{-1}$) promoted new tissue formation and the sprouting of capillary-like structures (Fig. 3*A*). In perfused cultures, we measured increases in cell numbers after 14 d in the chip (*SI Appendix*, Fig. S5*A*). The RFP-labeled ECs cultured with the MSCs and exposed to interstitial flow formed a densely interconnected network of vessels running through the tissue (Fig. 3*B*). Significant increases in vessel density, number of junctions, branching, and total vessel length, were measured in the perfused niches, supporting our hypothesis that physiologically relevant flow promotes the formation of a stable 3D microvasculature (Fig. 3*C*, *SI Appendix*, Fig. S5*B*, and Movie S5). Gene expression analysis demonstrated that cells exposed to flow had increased mRNA levels of the proangiogenic *POSTN* (periostin) and antiapoptotic *Survivin* markers (Fig. 3*D*). qRT-PCR performed on a mixed

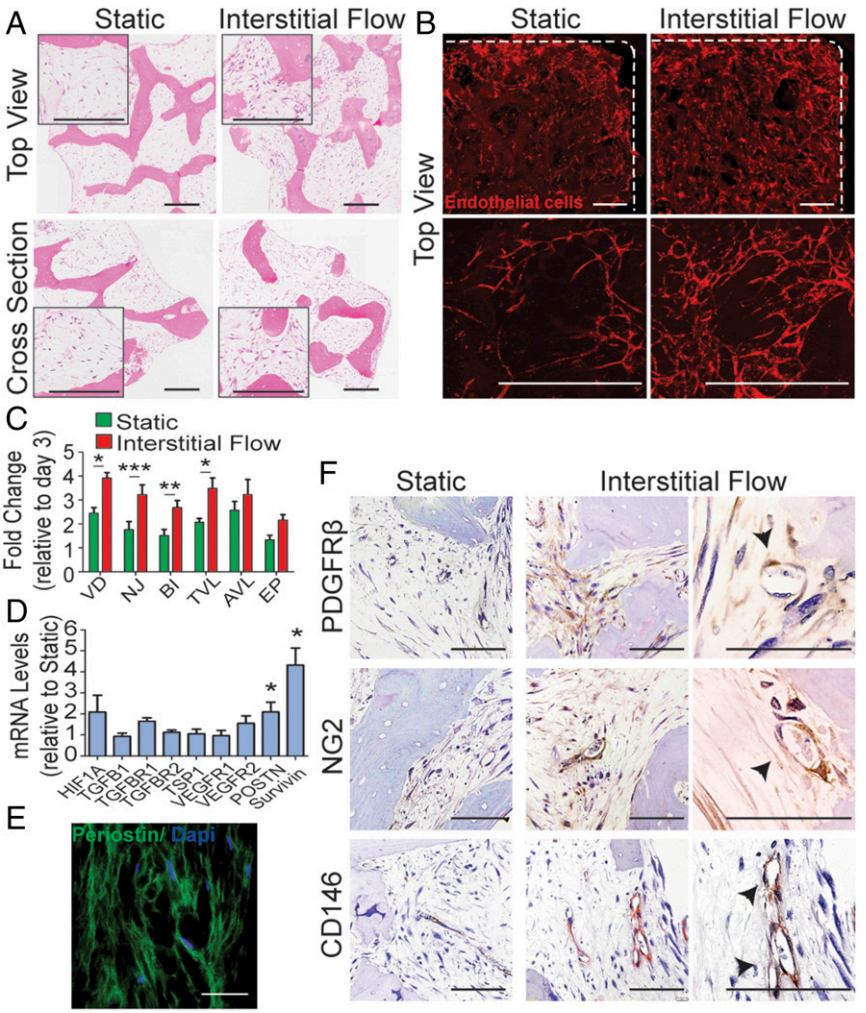

Fig. 3. Flow promotes vasculogenesis in the BoPV niche-on-a-chip. (*A*) *Top* view and cross-section of hematoxylin and eosin staining, showing newly formed tissue and capillary-like structures filling the trabecular spaces in the BoPV niche cultured statically or with interstitial flow (3.1 $\mu L \cdot s^{-1}$). (Scale bar: 250 μm.) Composite images were obtained by capturing and stitching high-magnification images. (*B*) Live confocal images showing RFP-labeled ECs in the BoPV niche and the static controls, after 2 wk of culture. (Scale bar: 350 μm.) (*C*) Quantification of vessel density (VD), number of junctions (NJ), branching index (BI), total vessel length (TVL), average vessel length (AVL), and number of endpoints (EP). Values were normalized to day 3. (*D*) Gene expression analysis; values were normalized to the static culture. (*E*) Immunofluorescence staining showing periostin deposited in the BoPV niche-on-a-chip. (Scale bar: 10 μm.) (*F*) Immunohistochemical analysis of perivascular markers in the static culture or in the BoPV niche-on-a-chip. Black arrowheads highlight the capillary-like lumens. (Scale bar: 100 μm.) Data in *C* and *E* are represented as average + SD; $n = 6$; $^*P < 0.05$, $^{**}P < 0.01$, $^{***}P < 0.001$, unpaired two-tailed Student's *t* test.

population of cells can give informative insights on the overall expression and not on the contribution of a single population of cells. However, immunofluorescence confirmed the secretion of periostin within the pores of the bone matrix (Fig. 3*E*). Periostin was not observed only in the proximity of RFP-expressing ECs, suggesting secretion by MSCs. Immunohistochemical staining showed that cells expressing the perivascular markers CD146, NG2, or PDGF-Rβ lined the vascular lumens and supported the formation of capillary-like structures (Fig. 3*F*). Overall, interstitial flow promoted cell proliferation and the formation of uniformly dense vascular networks, with cells forming capillary-like structures that expressed endothelial and perivascular markers.

Metastatic Colonization of the BoPV Niche-on-a-Chip. To simulate metastatic colonization, 250 breast cancer cells were introduced into each BoPV niche-on-a-chip and perfused, establishing a human triculture system. Using confocal microscopy, we tracked GFP-labeled MDA-MB-231 breast cancer cells and the RFP-labeled ECs (Fig. 4*A* and Movie S6). In static cultures, the cells formed only sparse vascular networks. In perfused cultures, the same cells self-assembled into dense vascular networks even in the presence of cancer cells. We observed a reduced number of cancer cells in the perfused niche after 1 wk of culture (Movie S7). To confirm this observation, breast cancer cells—expressing luciferase or GFP reporter gene—were cultured alone (C), with MSCs (C+M), or with MSCs and ECs (C+M+E) in the bone matrix, under flow or in static conditions. By quantifying the tumor cell area fraction normalized to day 7, we measured a fourfold decrease in cancer cell growth rate in perfused cultures (Fig. 4*B*). Using a luminescence assay, we supported these results (Fig. 4*C*). We confirmed that the reduction in cell concentration was not due to the cell loss into the flow. Instead, these results suggest that physiologically relevant interstitial flow triggered a slow-proliferative state in breast cancer cells colonizing the niche. Next, we investigated whether the receptor tyrosine kinase inhibitor sunitinib, commonly used to target proliferative cancer cells and vasculature, was effective in the BoPV niche-on-a-chip colonized by breast cancer cells. The drug concentration was set to 3.5 μM, the value corresponding to the half-maximal inhibitory concentration (IC_{50}) of sunitinib measured in monolayer cultures of breast cancer cells (*SI Appendix*, Fig. S5*C*). Cancer cell growth was inhibited by 50% following drug treatment in the absence of flow (Fig. 4*D*). Conversely, slow-proliferative cancer cells in the perfused niche were less sensitive to sunitinib treatment. There was no significant drop in cell number between sunitinib-treated and vehicle controls. Notably, we found that fluid flow in the BoPV niche-on-a-chip impaired growth and desensitized cancer cells to commonly used drugs. Overall, cancer cells colonized the BoPV niche-on-a-chip adapting to flow, ECM, and stromal cells. MSCs, mural cells, and ECs populated the niche and mediated metastatic homing. Anticancer drugs, targeting proliferating cancer cells and tumor vasculature, failed to affect the slow-proliferative cancer cells that were adapting and surviving in the niche (*SI Appendix*, Fig. S6).

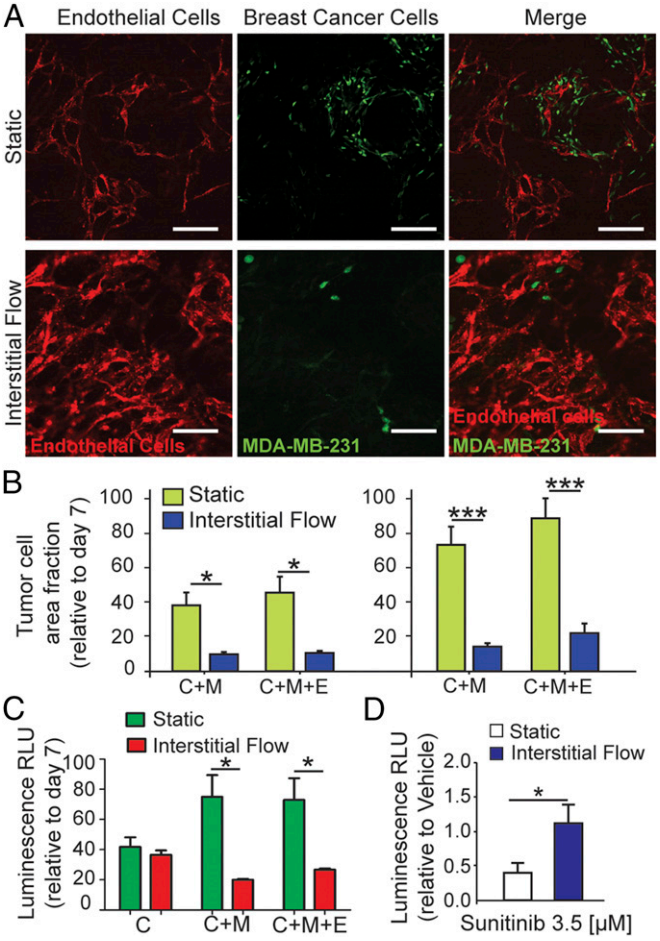

Fig. 4. Breast cancer cells colonization in the BoPV niche-on-a-chip. (*A*) Live confocal images of breast cancer cells (GFP-transduced MDA-MB-231 cells) in the BoPV niche with interstitial flow (~3.1 μm·s^{-1}; *Bottom*). (Scale bar: 50 μm.) (*B*) Tumor cell area fraction of GFP MBA-MB-231 breast cancer cells at days 10 and 14 in MSCs-only (C+M) or MSCs–ECs coculture (C+M+E) exposed to interstitial flow or cultured statically (no flow). Values were normalized to day 7 (1 d after cancer cells seeding). (*C*) Luciferase assay used to measure breast cancer cell growth within the bone niches containing only cancer cells (*C*), MSCs-only (C+M), or MSCs and ECs (C+M+E). Values were normalized to the luciferase signal at day 7 (1 d after cancer cells seeding into the tissue constructs). (*D*) The BoPV niches, infused with breast cancer cells, were treated with 3.5 μM sunitinib for 3 d. Luciferase assay was used to measure cancer cells survival. Values were normalized to the luciferase activity of tissue constructs treated with the drug vehicle (control). (*D*) Data in *B*–*D* are shown as average + SD; $n = 5$; $^{*}P < 0.05$, $^{***}P < 0.001$; unpaired two-tailed Student's *t* test.

Discussion

Microfluidic models aim to reconstitute functional units of organs that cannot be modeled easily in cell cultures or animals. In the context of cancer metastasis, these functional units can be conceived as niches where disseminated tumor cells colonize after extravasating the vascular route. By developing a BoPV niche-on-a-chip, we attempted to integrate some of the critical components of the metastatic cancer niche to model colonization. Our strategy differs from the well-established methodologies of culturing ECs with stromal cells on soft hydrogels, such as Matrigel or fibrin. Under these conditions, and in the presence of proangiogenic and progrowth mixtures, ECs form dense microvasculature. However, mimicking metastatic colonization under growth-promoting conditions may be misleading because cancer cells are constantly forced into highly proliferative states. Using a 3D bone matrix with its native features, we maintained EC viability and branching without the need of specialized culture mediums. While many of the culture systems used in previous studies were microfluidic in the sense that the channels used to insert and host the cells were of microscopic thickness, the culture medium and hydrogels carrying the cells were inserted into the device and maintained in nonperfused culture (17). Under nonperfused conditions, both the convective transport of soluble factors to cells and fluid-dynamic stimulation of the cells are absent. Thus, progressive oxygen drop and metabolic waste accumulation are not controlled, while important paracrine signals released by cells may reach only small distances due to diffusion barriers. To overcome these issues, flow velocities in the chip were adjusted using a computational model and

maintained at physiologically relevant levels (18). In addition, shear forces, which are crucial for tissue morphogenesis and vascular sprouting, depend on flow velocity and niche topology (4, 19). In vivo measurements of oxygen tension have shown the presence of steep oxygen gradients in the bone marrow, where arteries carry oxygen, nutrients, and growth factors into the interstitial space, before feeding into sinusoids, to form the venous circulation. In our chip, we mimic this function and show that similar oxygen gradients form in the direction of perfusion flow in the bone tissue. Mimicking interstitial flow, rather than blood flow, in the BoPV niche-on-a-chip, led to the formation of stable and dense vascular networks with capillary-like structures. However, it is unclear whether these vessels can accommodate flow. By showing blood vessels perfusability (i.e., introducing fluorescent dyes), this model will enable the study of additional steps of the metastatic cascade, including arrest in the blood stream and extravasation. Notably, perivascular cells expressing PDGF receptor-β, NG2, or CD146 wrap around the lumens of capillary-like structures formed by ECs. Mesenchymal stroma is heterogeneous and it is still debated whether mural cells, such as pericytes, originate from it. It is likely that, in our model, the perivascular cells originate from the MSCs. In healthy tissues, pericytes expressing, among others, specific markers such as PDGF-Rβ and NG2 are in close contact with ECs to create and remodel blood vessels. In primary tumors, pericytes act as gatekeepers against cancer extravasation; however, their role in cancer metastatic colonization is not clear (20). Early step of metastasis (intravasation, survival, arrest, extravasation) can be highly efficient (21). However, only a small subset of cells colonize and form macrometastases. To mimic colonization in the BoPV niche-on-a-chip, we infused 250 breast cancer cells into each bone tissue containing more than one million cells. Cancer cells that successfully engrafted grew readily in the absence of flow. Importantly, cancer cell proliferation rate decreased fourfold when exposed to interstitial flow. In contrast with some reports in the literature (6), in our model ECs have less effect on the cancer cell growth rate than the MSCs. Because this slow growth rate could have important implications on the inhibitory efficacy of small molecules, we studied the drug sensitivity of cancer cells engrafted in the BoPV niche-on-a-chip. We used sunitinib, which is an inhibitor of receptor tyrosine kinases that in breast cancer patients targets the tumor vasculature and proliferative cancer cells. Consistent with other reports, our data show that sunitinib inhibited breast cancer cell proliferation in 2D culture and in the statically cultured BoPV niche. However, sunitinib fails to affect slow-proliferative breast cancer cells disseminated in the BoPV niche-on-a-chip under perfusion, consistent with data collected in vivo. Studies in mice showed that sunitinib treatment was effective in inhibiting the primary tumors but increased the incidence of bone micrometastases (22). Experimental models and clinical studies both indicate that cancer stem cells survive many commonly employed anticancer molecules, including sunitinib (23). An attractive hypothesis is that cancer cells displaying stem cell features can successfully colonize distant organs and adapt to the changed niche microenvironment. When exposed to fluid-derived shear forces, oxygen gradients, stromal cells, and immune cells, these cells may be able to escape targeted therapy by entering in a slow-proliferative state.

In summary, we synergistically integrated fundamental components of the BoPV niche that may play a role in breast cancer metastatic colonization. Our microfluidic chip, in contrast to most other microfluidic systems, supports the cultivation of macroscopic tissues through precisely controlled flow, allowing live assessment of tissue development and vascularization over long periods of culture (weeks at the time). By introducing immune cells, tracking and quantifying their activity, this BoPV niche-on-a-chip could also become a powerful tool to design and test effective immunotherapy strategies in a physiologically relevant context. Modeling the early events of metastatic colonization using microfluidic chips may be useful to identify the key players mediating cancer latency toward designing more effective therapeutic strategies.

Methods

Cell culture, microfluidic chip, computational modeling, drug studies, and other standard techniques are described in *SI Appendix, SI Methods*. For niche-on-a-chip cultures, ECs expressing RFP were mixed with bone marrow MSCs and seeded into decellularized bone matrix. The coculture was maintained for 1 wk in the EM followed by 1 wk of microfluidic chip culture. After 6 d, MDA-MB-231/GFP or MDA-MB-231/Luc cells were suspended in DMEM with 1% FBS and 1% penicillin–streptomycin and added to the niche. For drug studies, 3.5 μM sunitinib was added to the culture. Cancer cell growth was assessed over 2 wk of culture. Only commercially obtained human cells were used in the experiments.

ACKNOWLEDGMENTS. We gratefully acknowledge funding of this work by NIH Grants EB002520 and EB17103 (to G.V.-N.) and the European Research Council Grant 646990-NICHOID (to M.T.R.).

1. Janni W, et al. (2011) Persistence of disseminated tumor cells in the bone marrow of breast cancer patients predicts increased risk for relapse—a European pooled analysis. *Clin Cancer Res* 17:2967–2976.
2. Braun S, et al. (2005) A pooled analysis of bone marrow micrometastasis in breast cancer. *N Engl J Med* 353:793–802.
3. Nguyen DX, Bos PD, Massagué J (2009) Metastasis: From dissemination to organ-specific colonization. *Nat Rev Cancer* 9:274–284.
4. Rutkowski JM, Swartz MA (2007) A driving force for change: Interstitial flow as a morphoregulator. *Trends Cell Biol* 17:44–50.
5. Calabrese C, et al. (2007) A perivascular niche for brain tumor stem cells. *Cancer Cell* 11:69–82.
6. Ghajar CM, et al. (2013) The perivascular niche regulates breast tumour dormancy. *Nat Cell Biol* 15:807–817.
7. Cross VL, et al. (2010) Dense type I collagen matrices that support cellular remodeling and microfabrication for studies of tumor angiogenesis and vasculogenesis in vitro. *Biomaterials* 31:8596–8607.
8. Polacheck WJ, German AE, Mammoto A, Ingber DE, Kamm RD (2014) Mechanotransduction of fluid stresses governs 3D cell migration. *Proc Natl Acad Sci USA* 111: 2447–2452.
9. Jeon JS, et al. (2015) Human 3D vascularized organotypic microfluidic assays to study breast cancer cell extravasation. *Proc Natl Acad Sci USA* 112:214–219.
10. Bersini S, et al. (2014) A microfluidic 3D in vitro model for specificity of breast cancer metastasis to bone. *Biomaterials* 35:2454–2461.
11. Wang J, Kazakia GJ, Zhou B, Shi XT, Guo XE (2015) Distinct tissue mineral density in plate- and rod-like trabeculae of human trabecular bone. *J Bone Miner Res* 30:1641–1650.
12. Galie PA, et al. (2014) Fluid shear stress threshold regulates angiogenic sprouting. *Proc Natl Acad Sci USA* 111:7968–7973.
13. Polacheck WJ, Charest JL, Kamm RD (2011) Interstitial flow influences direction of tumor cell migration through competing mechanisms. *Proc Natl Acad Sci USA* 108: 11115–11120.
14. Parmar K, Mauch P, Vergilio JA, Sackstein R, Down JD (2007) Distribution of hematopoietic stem cells in the bone marrow according to regional hypoxia. *Proc Natl Acad Sci USA* 104:5431–5436.
15. Ceradini DJ, et al. (2004) Progenitor cell trafficking is regulated by hypoxic gradients through HIF-1 induction of SDF-1. *Nat Med* 10:858–864.
16. Raimondi MT, Giordano C, Pietrabissa R (2015) Oxygen measurement in interstitially perfused cellularized constructs cultured in a miniaturized bioreactor. *J Appl Biomater Funct Mater* 13:e313–e319.
17. Zervantonakis IK, et al. (2012) Three-dimensional microfluidic model for tumor cell intravasation and endothelial barrier function. *Proc Natl Acad Sci USA* 109: 13515–13520.
18. Chary SR, Jain RK (1989) Direct measurement of interstitial convection and diffusion of albumin in normal and neoplastic tissues by fluorescence photobleaching. *Proc Natl Acad Sci USA* 86:5385–5389.
19. Song JW, Munn LL (2011) Fluid forces control endothelial sprouting. *Proc Natl Acad Sci USA* 108:15342–15347.
20. Cooke VG, et al. (2012) Pericyte depletion results in hypoxia-associated epithelial-to-mesenchymal transition and metastasis mediated by met signaling pathway. *Cancer Cell* 21:66–81.
21. Cameron MD, et al. (2000) Temporal progression of metastasis in lung: Cell survival, dormancy, and location dependence of metastatic inefficiency. *Cancer Res* 60:2541–2546.
22. Ebos JM, et al. (2009) Accelerated metastasis after short-term treatment with a potent inhibitor of tumor angiogenesis. *Cancer Cell* 15:232–239.
23. Conley SJ, et al. (2012) Antiangiogenic agents increase breast cancer stem cells via the generation of tumor hypoxia. *Proc Natl Acad Sci USA* 109:2784–2789.